# Alfvén cascade modes at high $\beta$ in the National Spherical Torus Experiment

N. A. Crocker,[1] E. D. Fredrickson,[2] N. N. Gorelenkov,[2] G. J. Kramer,[2] D. S. Darrow,[2] W. W. Heidbrink,[3] S. Kubota,[1] F. M. Levinton,[4] H. Yuh,[4] J. E. Menard,[2] B. P. LeBlanc,[2] and R. E. Bell[2]
[1]*University of California, Los Angeles, California 90095, USA*
[2]*Princeton Plasma Physics Laboratory, Princeton, New Jersey 08543, USA*
[3]*University of California, Irvine, California 92697, USA*
[4]*Nova Photonics, Princeton, New Jersey 08543, USA*

(Received 22 July 2008; accepted 12 September 2008; published online 7 October 2008)

Alfvén cascade (AC) modes are observed in the National Spherical Torus Experiment [M. Ono *et al.*, Nucl. Fusion **40**, 557 (2000)] reversed shear plasmas over a wide range (up to ~25% on axis, or ~11% at minimum $q$) of $\beta$ (ratio of kinetic pressure to magnetic pressure). At low $\beta$, the AC mode spectrum shows characteristics similar to conventional tokamaks. At higher $\beta$, distinct $\beta$ and $\nabla\beta$ effects are observed in the spectrum, including a significant reduction in the relative size of the frequency sweep and a toroidal mode number dependence in the minimum mode frequency. AC mode structure is obtained using reflectometry. Fast-ion loss associated with AC mode activity is observed. AC mode polarization at the plasma edge is consistent with expectation. Magnetohydrodynamic (MHD) spectroscopy is shown to be usable to determine $q_{\min}$ at both low $\beta$ and high $\beta$. Observed AC mode structure and frequency are found to be consistent with calculations for the same plasma conditions and geometry using the linear, ideal MHD hybrid kinetic code NOVA-K [C. Z. Cheng, Phys. Rep. **211**, 1 (1992)]. © *2008 American Institute of Physics*.
[DOI: 10.1063/1.2993182]

## I. INTRODUCTION

Recent results in the National Spherical Torus Experiment[1] (NSTX) extend the study of Alfvén cascade (AC) modes—also known as reversed-shear (RS) Alfvén eigenmodes (AEs)—to the relatively unexplored regimes of high $\beta$ (ratio of kinetic pressure to magnetic pressure) and high $\varepsilon$ (ratio of minor radius to major radius). The importance of AC modes derives from their significance in reversed-shear plasma operation, an advanced tokamak operation scenario planned for both ITER[2,3] and the Component Test Facility.[3] AC modes not only play a diagnostic role in RS plasmas, they directly impact plasma performance. AC modes have been shown to contribute to enhanced loss of beam-ions in both in the JT-60U[4,5] and DIII-D tokamaks.[6,7]

Alfvén cascade modes are shear Alfvén eigenmodes ($\omega \approx k_{\|} V_A$, neglecting $\beta$ and $\nabla\beta$ effects) that are excited by fast ions (e.g., fusion $\alpha$'s, beam ions, and ions accelerated by ion-cyclotron RF heating). They occur in RS plasmas, and are localized in minor radius to where the safety factor profile reaches its minimum value $q_{\min}$. They have been well studied experimentally in many conventional tokamaks (low $\beta$ and low $\varepsilon$), including JT-60U,[8] the Joint European Tokamak,[9] the Tokamak Fusion Test Reactor,[10] Alcator C-Mod,[11] and DIII-D.[12] In these studies, AC modes have been shown to play two important roles in RS plasmas. First, they directly impact plasma performance. AC modes can alter fast-ion orbits, leading to fast-ion transport and loss. Fast ions not only play critical roles in both plasma heating and current drive, they can cause damage to plasma facing components if they escape the plasma. Second, AC modes perform a diagnostic function. AC mode frequency is very sensitive to the value of $q_{\min}$, so small changes in $q_{\min}$ cause significant sweeping of the mode frequency. This sensitivity allows a relatively precise determination of $q_{\min}$ from AC mode frequency, a technique referred to as magnetohydrodynamic spectroscopy (MHD).[9,13,14]

In contrast with the long history of reports of AC mode observations in conventional tokamaks, reports of observations in spherical tori have emerged only relatively recently. Consequently, AC modes have been studied relatively little at high $\beta$ and high $\varepsilon$. The first reported observations of AC modes in a spherical torus were in the Mega-Ampère Spherical Torus (MAST),[15] followed shortly thereafter by observations in NSTX.[16] Although the MAST observations advanced the study of AC modes into a new regime of high $\beta$ and high $\varepsilon$, the analysis of those observations gave little consideration to the implications of high $\beta$ and high $\varepsilon$ for AC mode phenomenology. In contrast, the NSTX report focused on aspects of AC mode phenomenology peculiar to high $\beta$ plasma operation, including $\beta$-induced suppression of AC modes and the effects of $\beta$ on the AC mode frequency.

NSTX—with a major radius of $R=1.0$ m, a minor radius of $a=0.65$ m, and an inverse aspect ratio of $\varepsilon \equiv a/R=0.65$—is well suited to the study of AC modes in the regime of high $\beta$ and high $\varepsilon$. First, AC modes have been observed in NSTX plasmas with central plasma toroidal betas of up to $\beta_{T0} \sim 25\%$, which is much higher than can be achieved in conventional tokamaks ($\beta_{T0} \lesssim 5\%$). (The value of $\beta_T$ is the ratio of the total kinetic pressure—including thermal pressure and the contribution from fast ions, as dis-

 

cussed in Sec. III—to the volume average pressure of the vacuum toroidal magnetic field.) Second, reverse-shear operation has been independently verified in NSTX using the motional Stark effect (MSE) diagnostic.[17,18] The MSE capability is critical in the study of AC modes, since the spectrum and characteristics of fast-ion modes are very sensitive to the shear in the equilibrium magnetic field of the plasma. Finally, NSTX is capable of achieving, and in fact typically operates at $\beta_{T0}$ much higher than 25%, where AC modes have not been observed, despite verified shear reversal.[16] The regime of high $\beta$ near the threshold for suppression of AC modes is of particular interest in the study of AC modes.

The analytic theory of Alfvén cascade modes has focused on the regime of low inverse aspect ratio and low $\beta$.[19–24] In part, this is because this regime allows approximations that make the analytic theory more tractable. It is also because this regime is appropriate for conventional tokamaks, in which nearly all experimental observations of AC modes have occurred. However, this regime is not appropriate to a spherical torus such as NSTX. In order to treat AC modes at the high inverse aspect ratio and high $\beta$ that are relevant to spherical tori, it is necessary use codes such as NOVA-K.[25–27] NOVA-K is a linear, ideal MHD hybrid kinetic code that calculates Alfvén eigenmode frequency, structure, and growth rate. It employs realistic toroidal plasma geometry, making it useful for spherical tori, as well as conventional tokamaks. It treats the fast-ion population perturbatively in order to assess the effect of fast ions on mode growth rates. It also includes the acoustic coupling of Alfvén eigenmodes that results from compressibility due to geodesic field line curvature when $\beta$ is nonvanishing.[22] NOVA-K includes "Chu filtering" to remove acoustic singularities.[28]

The results reported here include observations of AC mode spectra and structure in NSTX reversed shear plasmas over a range of $\beta$, including values much higher than achievable in conventional tokamaks. It includes observations of fast-ion loss associated with AC mode activity, measurements of mode structure obtained via fixed frequency reflectometers and AC mode polarization at the plasma edge. It also considers the application of MHD spectroscopy in spherical tori, both at low values of $\beta$ ($\beta_T \sim 6\%$) that are at the high end of what is achievable in conventional tokamaks and at higher values of $\beta$ ($\beta_T \sim 11\%$) that are, nonetheless, at the low end of the range achievable in spherical tori. Experimental observations of AC mode structure and frequency are shown to be consistent with NOVA-K calculations for the same plasma conditions and geometry.

This report is organized into seven sections, including this one. Section II describes NSTX and the experimental conditions. Section III presents experimental observations, including AC mode spectra over a range of $\beta$, a measurement of AC mode polarization, and observations of fast-ion transport associated with AC mode activity. Section IV presents an analysis of the $\beta$ dependence of the AC mode spectrum and examines the applicability of MHD spectroscopy over the range of $\beta$ considered. Section V presents a comparison of an experimentally observed AC mode with a calculation of mode frequency and structure using NOVA-K. Beyond this comparison, other conclusions arising from the NOVA-K calculation are discussed. The report finishes with a discussion of the results in Sec. VI and a summary of the results and conclusions in Sec. VII.

## II. EXPERIMENTAL CONDITIONS

The results reported here are obtained in L-mode plasmas with a major radius of $R=1.0$ m and a minor radius of $a=0.65$ m. These plasmas have a lower-single-null geometry with an elongation of $\kappa \sim 1.9$ and a triangularity of $\delta \sim 0.35$. They are fueled with helium gas puffing and are both heated and fueled with 2 MW of power injected by a 90 keV neutral beam. Two different beam sources—source A, with a tangency major radius of $R_{\tan}=69.4$ cm and source C with $R_{\tan}=49.7$ cm—are used at different times. Source A is specifically needed to obtain MSE measurements, but source C is also used since source A tends to excite rapid frequency chirps which can break up and obscure the frequency sweep of Alfvén cascade modes. TRANSP modeling[29,30] indicates the resulting plasmas are predominantly fully stripped helium ($n_{\mathrm{He}}/n_{\mathrm{D}} > 1$), taking into account the measured D-D fusion neutron rate and using carbon density obtained from the charge exchange recombination spectroscopy (CHERS) diagnostic[31,32] to calculate $Z_{\mathrm{eff}}$. The external toroidal magnetic field ($B_{T0}$) is 4.5 kG in vacuum at $R=1.0$ m for some plasmas and 5.5 kG for others. The toroidal plasma current is ramped to 0.8 MA in the first ~0.25 s of each discharge and held steady thereafter until plasma termination. Figure 1(a) illustrates the time evolution of plasma current ($I_p$) and injected beam power in a typical plasma (shot 123810). In order to study the $\beta$ dependence of Alfvén cascade modes, plasmas with varying electron density are created by adjusting the helium puffing. The peak value of electron density ($n_{e0}$), measured with multipoint Thomson scattering (MPTS),[33] ranges from ~1 to $3.5\times10^{19}$ m$^{-3}$. The electron temperature, also measured with MPTS, varies as well, with peak values ($T_{e0}$) ranging from ~0.5 to 1.5 keV. The time evolution of $n_{e0}$ and $T_{e0}$ for a typical plasma is illustrated in Fig. 1(b). (The particular plasma illustrated, i.e., shot 123810, has $B_{T0}=5.5$ kG.) As is typical for L-mode operation, the plasmas have strongly centrally peaked density and temperature profiles. Density and temperature profiles for a typical plasma (shot 123810) are illustrated in Fig. 1(c). For these conditions, Alfvén speed $V_A$ ranges from $\sim 1.2\times10^6$ to $\sim 2.7\times10^6$ m/s at the magnetic axis and the relative speed of the 90 keV beam ions, given by $V_{\mathrm{beam}}/V_A$, ranges from ~0.8 to ~1.8.

## III. EXPERIMENTAL RESULTS

Alfvén cascade modes are observed in the plasmas described above. Figure 2 shows a spectrogram for a typical low density, low $\beta$ NSTX plasma (shot 120103) obtained with a Mirnov coil positioned outside the plasma.[16] Toroidal mode numbers are identified for the evolving modes using a toroidally distributed array of such coils. The peak electron density remains nearly constant at $n_{e0} \sim 1.2\times10^{19}$ m$^{-3}$ over the period shown in the figure, and the peak electron temperature $T_{e0}$ increases from ~0.6 to ~1.4 keV. At $t=0.271$ s, $\beta_T \sim 6\%$ at $R=1.25$ m, which is the location of

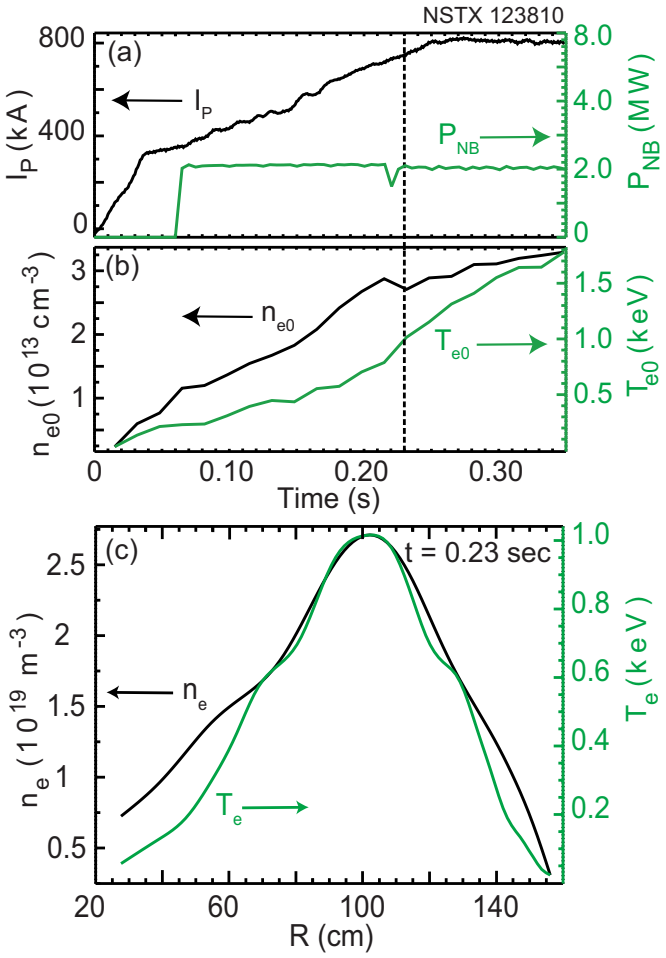


FIG. 1. (Color online) Time evolution in a typical plasma of (a) plasma current $I_p$, neutral beam power $P_{NB}$, and (b) central electron density and temperature, $n_{e0}$ and $T_{e0}$, respectively. (c) Typical profiles of $n_{e0}$ and $T_{e0}$ vs major radius $R$ near end of current ramp ($t$=0.230 s).

minimum $q$ determined for several similar plasmas for which MSE is available. Included in the value of $\beta_T$ is the contribution from fast ions (which is substantially greater than the thermal contribution at the location of minimum $q$ for the conditions of Fig. 2) determined via TRANSP modeling using a Monte Carlo treatment of the beam ions. The ion thermal contribution is calculated from the ion density and ion temperature. As discussed in Sec. II, the ion density is also determined via this TRANSP modeling. The ion temperature is assumed to be equal to the carbon ion temperature (typically, $\sim T_e/2-T_e$) measured by the CHERS diagnostic. The electron thermal contribution is determined using the electron density and temperature measurements obtained with the MPTS diagnostic. The spectrum illustrated in Fig. 2 shows sequences of large, upward frequency sweeps with sequential toroidal modes numbers. The large upward frequency sweeps identify these modes as Alfvén cascade modes (an identification supported by further analysis discussed below). Such sequences are characteristic for Alfvén cascade modes at low $\beta$ and are commonly observed in conventional tokamaks.[8–12]

Figure 3(a) illustrates an edge Mirnov spectrogram for a plasma (shot 120118) with a higher $\beta$ and higher density than that in Fig. 2.[16] Toroidal mode numbers in this

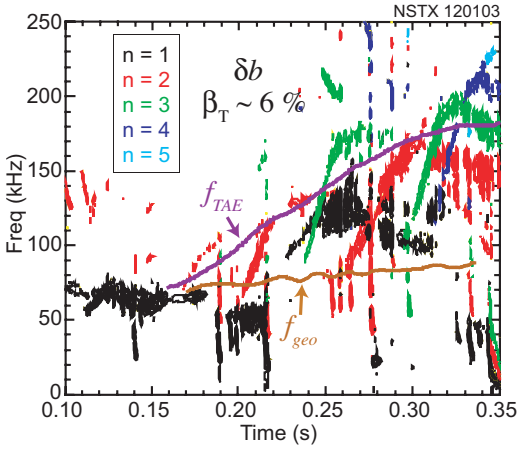


FIG. 2. (Color) Edge Mirnov spectrogram for a typical low density, low $\beta$ NSTX plasma (shot 120103: $\beta_T \sim 6\%$ at $R$=1.25 m, $t$=0.271 s). Colors identify toroidal mode numbers (Ref. 16).

moderate $\beta$ plasma are identified for each mode in the spectrogram. The peak electron density and temperature for this plasma increase over the time period shown from $n_{e0} \sim 2.0\times10^{19}$ m$^{-3}$ and $T_{e0} \sim 0.6$ keV to $n_{e0} \sim 3.5\times10^{19}$ m$^{-3}$ and $T_{e0} \sim 1.4$ keV. At $t$=0.271 s, $\beta_T \sim 11\%$ at $R$=1.25 m, which is the location of minimum $q$ determined in a similar plasma using MSE data. The $n$=2–5 modes in Fig. 3(a) can be seen to begin upward frequency sweeps at $t \sim 0.22$, 0.24, 0.26, and 0.28 s, respectively. These upward sweeps are identified as Alfvén cascade modes. Notably, the frequency range covered by these sweeps is proportionately much smaller [i.e., $\Delta\omega/\max(\omega)$ is much smaller] than that for the AC modes in the low $\beta$ plasma illustrated in Fig. 2. As will be discussed below, this change is consistent with predicted

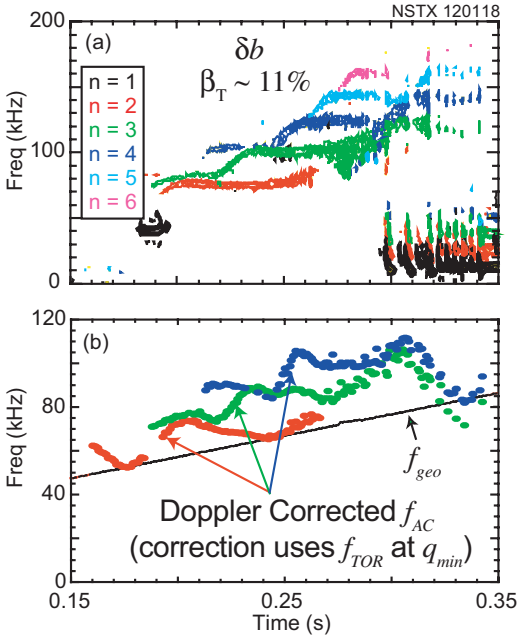


FIG. 3. (Color) (a) Edge Mirnov spectrogram for a typical moderate density, moderate $\beta$ NSTX plasma (shot 120118: $\beta_T \sim 11\%$ at $R$=1.25 m, $t$=0.271 s). Colors identify toroidal mode numbers. (b) Doppler corrected frequencies of the spectral peaks appearing in (a) (Ref. 16).

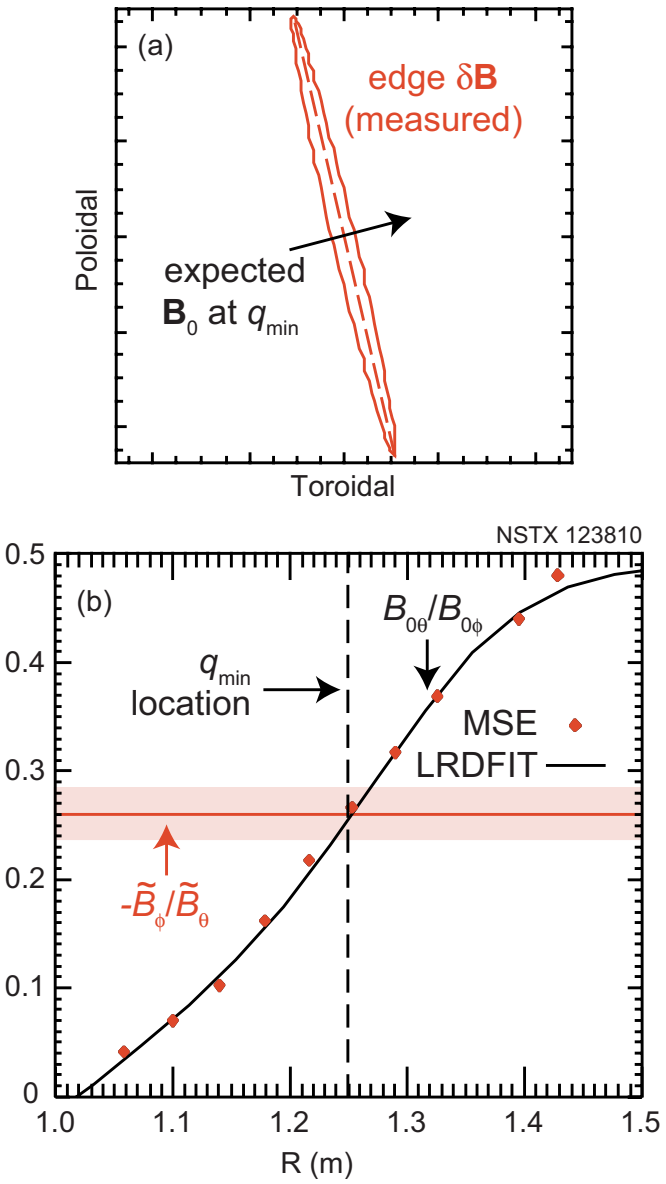


FIG. 4. (Color online) (a) $\delta B_\phi$ vs $\delta B_\theta$ (—) for one cycle of the $n=2$ AC mode (see Fig. 3), with major axis (– –) and direction (→) of $\mathbf{B}_0$ expected at the location of minimum $q$; magnitude of $\delta B \sim 0.6$ G. (b) Comparison of equilibrium pitch $B_{\theta 0}/B_{\phi 0}$ from LRDFIT (—), constrained by MSE measurements (♦), with pitch required for $\mathbf{B}_0 \perp \delta\mathbf{B}$, which is given by $-\delta B_\phi/\delta B_\theta$ (horizontal line). Experimental uncertainty (horizontal band) of $-\delta B_\phi/\delta B_\theta$ and location of minimum $q$ also shown (– –).

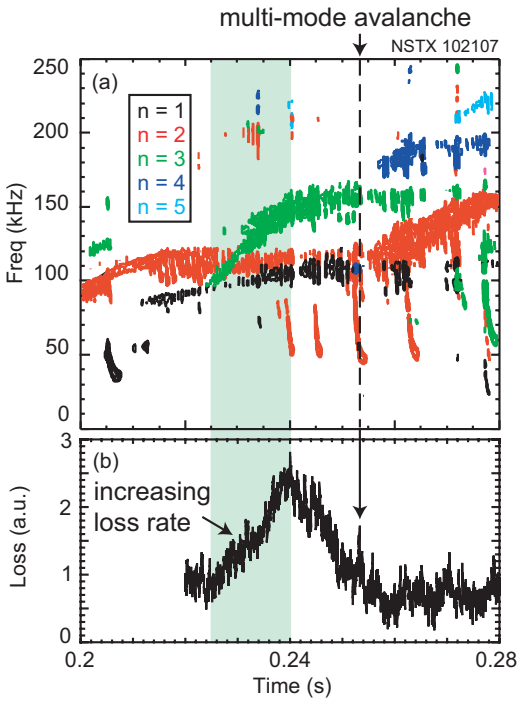


FIG. 5. (Color) (a) Edge Mirnov spectrogram for a moderate density, low $\beta$ NSTX plasma (shot 120107) and (b) fast-ion loss rate measured by sFLIP. Multimode avalanche event and period of increasing loss rate are shown by annotations.

$\beta$ and $\nabla\beta$ effects[34,22–24] on the Alfvén cascade mode frequency. Figure 3(b) shows the Doppler corrected frequencies for several of the modes. The Doppler correction is determined using the carbon toroidal rotation velocity measured at $R=1.25$ m by the CHERS diagnostic.

Figure 4(a) illustrates the edge magnetic fluctuation $\delta\mathbf{B}$ of an $n=2$ AC mode in the low $\beta$ plasma of Fig. 1 at $t=0.230$ s ($\beta_T \sim 3\%$ at $R=1.25$ m), midway through the mode's frequency upsweep. The magnitude of $\delta\mathbf{B}$ at the time shown is ~0.6 G. (It is typically ~0.1 G throughout the AC mode frequency upsweep, with occasional bursts such as at the time shown.) The figure shows $\delta B_\phi$ versus $\delta B_\theta$ over one cycle of the mode. The major axis of the resulting ellipse indicates the orientation, or polarization, of $\delta\mathbf{B}$ in the poloidal-toroidal plane at the plasma edge. It is apparent, of course, that $\delta B_\phi$ and $\delta B_\theta$ are not perfectly in phase, or the ellipse would be a straight line. However, the relative phase is zero within experimental uncertainty. Also shown is a vector perpendicular to the major axis of the ellipse that illustrates the expected orientation of the equilibrium $\mathbf{B}_0$ for a shear Alfvén wave with the measured $\delta\mathbf{B}$. Since the AC mode is essentially a shear Alfvén wave radially localized to the weak-shear region at the location minimum of $q$, it is expected that the equilibrium $\mathbf{B}_0$ there will be oriented in the direction indicated by the vector. Figure 4(b) shows this to be the case. The figure shows $B_{\theta 0}/B_{\phi 0}$, the equilibrium magnetic field pitch measured by MSE, versus the major radius. It also shows the measured value of $-\delta B_\phi/\delta B_\theta$ (with experimental uncertainty), which indicates the value of $B_{\theta 0}/B_{\phi 0}$, for which $\mathbf{B}_0 \perp \delta\mathbf{B}$. The location of minimum $q$ is also indicated in the figure. It is apparent that the condition $-\delta B_\phi/\delta B_\theta = B_{\theta 0}/B_{\phi 0}$ is satisfied very close to the location of minimum $q$. Interestingly, the value of $-\delta B_\phi/\delta B_\theta$ is constant to within ~15% throughout AC mode's frequency upsweep. While an AC mode is essentially a shear Alfvén wave for most of its frequency upsweep, including at the time shown in Fig. 4, it experiences significant acoustic coupling (discussed in Sec. IV, below) near the beginning of the upsweep, which might be expected to modify its polarization in some way. However, there appears to be no evidence for any such modification in this case.

Measurements with the scintillator Fast Lost-Ion Probe[35] (sFLIP) indicate that AC modes play a role in loss of fast-ions from the plasma. Figure 5(a) shows a spectrogram from an edge Mirnov coil in a low $\beta$ plasma (shot 120107) show-

ing the evolution of several modes (toroidal mode numbers indicated by different colors). Figure 5(b) shows fast-ion loss rate measured by sFLIP plotted for the same time period as in Fig. 5(a). The loss rate can be seen to increase with time over the period $t=0.225-0.240$ s. From Fig. 5(a), it can be seen that this period corresponds to the upward frequency sweep of the $n=3$ (green) AC mode. Near the end of the sweep, around $t=0.240$ s, the loss rate begins to decrease again. The timing of the increase and subsequent decrease indicate that the $n=3$ AC mode plays a role in the increased loss. (Interestingly, observations reported in Ref. 5 showed the degradation of fast-ion confinement due to AC modes to be most severe at the end of the frequency upsweep.) In addition to the correlation of the loss rate with the existence of the $n=3$ AC mode, it can also be seen in Fig. 5 that AC modes participate in multimode loss events.[36,37] At $t=0.253$ s, a spike in the loss rate can be seen in Fig. 5(b). There is also a sudden simultaneous ~4% drop in the flux of D-D fusion neutrons from the plasma (not shown) at $t=0.253$ s, indicating a sudden loss or redistribution of fast ions. The spike in the loss rate and the drop in the neutron production rate coincides with the birth of the $n=2$ (red) AC mode, as can be seen in Fig. 5(a).

## IV. ANALYSIS

In low $\beta$ plasmas (e.g., in conventional tokamaks), the evolution of the Alfvén cascade mode spectrum is very distinct. Spectral peaks, typically occurring in clusters with sequential mode numbers, undergo large rapid (tens of milliseconds) upward frequency sweeps $[\Delta f/\max(f)\sim 1]$ that start near zero frequency. Each upwardly sweeping spectral peak is caused by an AC mode. The frequency sweeps saturate at the "TAE frequency," $f_{\mathrm{TAE}}=\omega_{\mathrm{TAE}}/(2\pi)=V_A/(4\pi q_{\min}R)$, where $V_A$ is the Alfvén velocity, given in terms of the magnetic field ($B$) and plasma mass density ($\rho$) by $V_A^2=B^2/\mu_0\rho$. As the frequency saturates, the AC mode converts "adiabatically" into a toroidicity-induced Alfvén eigenmode (TAE).[21]

The large rapid upward frequency sweep that an Alfvén cascade mode undergoes is a natural consequence of its localization near the minor radial location of minimum $q$, $r_{\min}$. At zero $\beta$, AC modes are approximately pure shear Alfvén waves, with a frequency given by

$$\omega \approx k_{\|}V_A \tag{1}$$

that can exist partly because of the weak shear $(\mathrm{d}q/\mathrm{d}r\sim 0)$ in the region around $r_{\min}$. An AC mode is an eigenmode with a toroidal number $n$ consisting of one dominant poloidal harmonic with mode number $m$ and sideband harmonics including, predominantly, $m\pm 1$. Consequently, for $\varepsilon\ll 1$, $k_{\|}\approx(m/q_{\min}-n)/R$. The frequency of an AC mode sweeps upward as $q_{\min}$ decreases (due, for instance, to the soak-in of the magnetic field during a ramp-up of inductively driven plasma current). The upward sweep starts when $q_{\min}$ passes through $m/n$. When $q_{\min}=m/n$, $k_{\|}=0$, so any subsequent decrease in $q_{\min}$ causes a relatively large change in frequency.

Both the pressure[22] and pressure gradient[34,23,24] can modify the Alfvén cascade mode frequency sweep. Plasma pressure plays a role because of geodesic field line curvature.[38] Taking into account plasma compressibility, geodesic field line curvature couples Alfvénic and acoustic oscillations, introducing an acoustic, or compressional, component to the AC mode perturbation. The influence of the pressure gradient, which can play a critical role in radial localization of the AC mode, is independent of this compressional effect. In a cold, uniform plasma with no magnetic shear, the shear Alfvén wave spectrum is degenerate with respect to perpendicular wavenumber (i.e., radial structure).[21] The weak shear region around $r_{\min}$ tends to create such degeneracy, but the pressure gradient, among other factors, can break the degeneracy.[34] Including both the pressure and pressure gradient effects, the AC mode dispersion relation expressed in Eq. (1) is modified, becoming

$$\omega^2 \approx k_{\|}^2V_A^2+\omega_{\mathrm{geo}}^2+\omega_{\nabla\beta}^2+\delta\omega^2, \tag{2}$$

where the $\omega_{\mathrm{geo}}^2=2\gamma P/\rho R^2$ is the contribution of the geodesic acoustic coupling, $\omega_{\nabla\beta}^2$ represents the contribution of the pressure gradient, and $\delta\omega^2$ represents other, typically small, effects. The symbols $\gamma$ and $\rho$ represent the plasma adiabatic index and mass density, respectively. It is important to note that, while $\omega_{\mathrm{geo}}^2$ is always positive and independent of $k_{\|}$, the same is not true for $\omega_{\nabla\beta}^2$, as will be discussed below.

The effects of geodesic acoustic coupling on AC mode frequency are fairly straightforward. One effect, as observed in many conventional tokamaks,[22,39–42] is the shift of the minimum AC mode frequency up from zero by $\omega_{\mathrm{geo}}$. The entire upward sweep occurs as $q_{\min}$ changes from $m/n$ to $(m-1/2)/n$. The value of $k_{\|}$ changes from 0 to $1/2q_{\min}$, so $(k_{\|}V_A)^2$ changes from 0 to $\omega_{\mathrm{TAE}}^2$. In sufficiently low $\beta$ plasmas, $\omega_{\mathrm{geo}}\ll\omega_{\mathrm{TAE}}$, so, neglecting $\omega_{\nabla\beta}$, a sweep starts at the geodesic frequency, $f_{\mathrm{geo}}=\omega_{\mathrm{geo}}/2\pi$, and ends at $\sim f_{\mathrm{TAE}}$. This is the sweep range typically observed in conventional tokamaks. Interestingly, this tendency seems to support the assumption that $\omega_{\nabla\beta}$ can, indeed, often be neglected there. This is perhaps not surprising since conventional tokamaks commonly operate in high confinement mode, or H-mode, when operating with reverse shear. In H-mode, $\beta/(a|\nabla\beta|)$ can be large at $r_{\min}$, suggesting that $\nabla\beta$ effects may be weak.

It is noteworthy that the spectrogram in Fig. 2, which shows the AC mode spectral evolution in a low $\beta$ plasma, shows many of the features observed in conventional tokamaks. The modes sweep upwards from $\sim f_{\mathrm{geo}}$ to $\sim f_{\mathrm{TAE}}$, both of which are indicated in the figure. The values shown for $f_{\mathrm{geo}}$ and $f_{\mathrm{TAE}}$ are calculated using plasma parameters at $R=1.25$ m, which is the location where $q$ is at a minimum. The expression used to calculate $f_{\mathrm{geo}}$, motivated by Ref. 22, is

$$\omega_{\mathrm{geo}}^2=(2Z_iT_e/m_iR^2)(1+7T_i/4Z_iT_e) \tag{3}$$

for a plasma with a single ion species of mass $m_i$ and charge $eZ_i$. (Reference 22 considers a single ion species with $Z_i=1$.) This expression accounts for kinetic effects, neglecting corrections of order $1/2q_{\min}^2$, which are small for the modes in question. (Any contribution fast-ion compressibility might make to $\omega_{\mathrm{geo}}$, an issue discussed in Sec. V below, is also

neglected.) The value for $f_{geo}$ shown in Fig. 2 is calculated assuming the ion species is $D^+$. If the ion species is $He^{2+}$, $f_{geo}$ is reduced, but only by ~20%, since $T_i \sim T_e$.

A second effect of geodesic acoustic coupling is that the relative size of the sweep $[\Delta\omega/\max(\omega)]$ is reduced as $\beta$ increases. Neglecting $\omega_{\nabla\beta}$ and $\delta\omega$, $\Delta\omega^2 = \omega_{TAE}^2$ and $\max(\omega^2) = \omega_{TAE}^2 + \omega_{geo}^2$. So, from Eq. (2), the relative size of the sweep is given by

$$\Delta\omega^2/\max(\omega^2) \approx \omega_{TAE}^2/(\omega_{TAE}^2 + \omega_{geo}^2) = (1 + 4\gamma\beta q_{min}^2)^{-1}, \quad (4)$$

where $\beta = 2P/\rho V_A^2$. This clearly decreases as $\beta$ increases. This effect is apparent when comparing the AC spectrum shown in Fig. 3 with the AC spectrum shown in Fig. 2. Figure 3 shows AC modes in a plasma with significantly higher $\beta$ than that of the AC modes shown in Fig. 2.

The effects of $\nabla\beta$ on the AC mode frequency[34,23,24] are somewhat more complicated than those of geodesic acoustic coupling. One effect is that the relative sweep size reduces as $|\nabla\beta|$ increases. The contribution of $\omega_{\nabla\beta}$ to AC mode frequency increases the minimum value and decreases the maximum value.[34,23,24] This effect may partially contribute to the change in relative sweep size from Fig. 2 to Fig. 3. The spectra shown in Fig. 2 and Fig. 3 are both obtained in L-mode plasmas with similarly shaped $\beta$ profiles. Consequently, as $\beta$ increases from Fig. 2 to Fig. 3, $|\nabla\beta|$ increases as well. Perhaps more interesting is that the contribution of $\omega_{\nabla\beta}^2$ to the minimum AC mode frequency varies with mode number. The contribution of $\omega_{\nabla\beta}^2$ is expected to shift the minimum frequency upward by an amount that grows as toroidal mode number increases.[34] This effect is consistent with the AC spectrum in Fig. 3. The geodesic frequency, $f_{geo}$ (black line), calculated assuming an ion species of $D^+$, is indicated in Fig. 3(b). [The value shown for $f_{geo}$ is actually reduced by a factor of 0.9 from the value predicted using Eq. (3) so that it agrees with the observed frequency minima of the $n=2$ mode. However, this adjustment is within experimental uncertainty, including, in particular, that due to the presence of an unknown, but substantial, amount of $He^{2+}$ in the plasma.] The value shown for $f_{geo}$ represents the expected minimum AC mode frequency in the absence of any contribution from $\omega_{\nabla\beta}^2$. As can be seen in Fig. 3(b), the minimum Doppler corrected mode frequency for each mode shifts farther upwards from $f_{geo}$ as toroidal mode number increases. This shift, which is, for instance, ~15 kHz for the $n=3$ mode, is well beyond the uncertainty in the Doppler corrected mode frequencies. The uncertainty due to the mode spectral width is ~1 kHz [comparable to the mode frequency plot symbol width in Fig. 3(b)], while the statistical uncertainty of the toroidal rotation measured near the location of minimum $q$ ($R=1.25$ m) is $\sim\frac{1}{2}$ kHz. This gives a combined uncertainty of ~1–2 kHz for the Doppler corrected $n=2$–4 mode frequencies. It should be noted, however, that there is another possible source of uncertainty, toroidal rotation shear. The toroidal rotation frequency increases at a rate of $\sim\frac{1}{2}$ kHz/cm as radius decreases for $R<1.25$ m. It is unclear what uncertainty this introduces, though, since the effects of rotation shear on AC modes are not well understood.

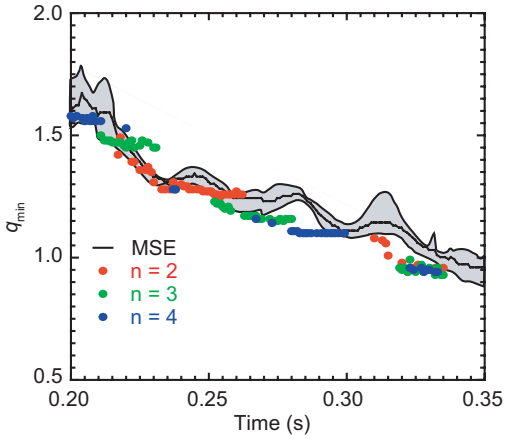


FIG. 6. (Color) $q_{min}$ reconstructed using $n=2$ (red), $n=3$ (green), and $n=4$ (blue). AC modes in a low $\beta$ plasma (shot 123099). Also shown is the average (—) and standard deviation (gray band) of $q_{min}$ determined using MSE measurements over several very similar plasmas.

It has become a common practice in diagnosing experiments in conventional tokamaks to use observed AC mode frequency sweeps to determine the evolution of $q_{min}$ over time.[9,13,14] This practice takes advantage of the sensitivity of the AC mode frequency to $q_{min}$, which, as noted above, can change by nearly 100% of its maximum value, in the limit of low $\beta$, as a result of a change in $q_{min}$ of just $1/2n$. This change in $q_{min}$ is typically quite small since, typically, $n \gg 1$. Furthermore, although AC mode frequency depends on other plasma parameters, not only it is comparatively insensitive to them, they change relatively little during the sweep.

MHD spectroscopy also proves to be usable in low $\beta$ NSTX plasmas such as those illustrated in Fig. 2. (See also Ref. 16.) Equation (2) may be rearranged to express $q_{min}$ in terms of the AC mode frequency $\omega$. Assuming $\delta\omega$ and $\omega_{\nabla\beta}$ are negligible, this gives

$$q_{min} \approx m/(n + \sqrt{\omega^2 - \omega_{geo}^2}/\omega_A), \quad \text{where } \omega_A = V_A/R. \quad (5)$$

It is possible, using Eq. (5), to determine $q_{min}$ from the observed AC mode frequency, given independent measurements of the mode numbers $n$ and $m$, and the characteristic frequencies $\omega_{geo}$ and $\omega_A$. Figure 6 shows $q_{min}$ reconstructed using several AC modes in a low $\beta$ plasma (shot 123099; $\beta_T \sim 6\%$ at $R=1.25$ m and $t=0.271$ s). The toroidal mode numbers for each of the modes (indicated by the different colors) are determined using the toroidally distributed array of Mirnov coils at the edge of NSTX. The poloidal mode numbers are chosen so that the reconstructed $q_{min}$ is consistent among the several modes observed. The values used for $\omega_{geo}$ and $\omega_A$ are determined from CHERS and MPTS data at the location of minimum $q$. Figure 6 also shows an average over several similar plasmas of $q_{min}$ determined using MSE measurements and LRDFIT.[17,18] (LRDFIT is a Grad–Shafranov equilibrium reconstruction code that uses an L-R circuit equation model of the plasma, vessel, and passive plate currents to better constrain the equilibrium fits. It self-consistently incorporates constraints from magnetics,

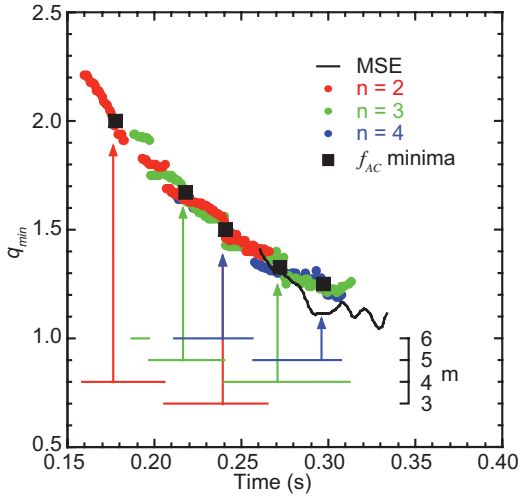


FIG. 7. (Color) $q_{\min}$ reconstructed using $n=2$ (red), $n=3$ (green), and $n=4$ (blue). AC modes in a moderate $\beta$ plasma (shot 120118; see Fig. 3). The poloidal mode numbers used for the reconstruction are indicated by the annotations. Also shown is $q_{\min}$ (—) determined using MSE measurements in a similar plasma (Ref. 16).

$E_r$-corrected MSE, $T_e$ isosurfaces, and density and pressure asymmetries from centrifugal effects in the equilibrium reconstructions.) The standard deviation of shot-to-shot variation of the $q_{\min}$ determined with MSE data is shown. As can be seen, the reconstruction from the AC modes is very similar to the value determined from the MSE data.

It is a question of significant interest whether MHD spectroscopy can also be applied in those higher $\beta$ plasmas in which AC modes are observed and in which $\omega_{\text{geo}}$ approaches $\omega_{\text{TAE}}$. Furthermore, it is important to determine whether it can be applied when the contribution of $\omega_{\nabla\beta}^2$ is significant. MHD spectroscopy becomes more complicated in such plasmas because $\omega_{\nabla\beta}^2$ depends on $k_\parallel$. The AC spectrum shown in Fig. 3 allows both questions to be addressed. In order to reconstruct $q_{\min}$ from mode frequency, some knowledge of the relationship between $k_\parallel$ and $\omega_{\nabla\beta}^2$ is required. Unfortunately, little guidance is provided in the literature for the high $\beta$ and high $\varepsilon$ conditions of Fig. 3. However, Refs. 23 and 24 indicate that, in the limit of low $\beta$ and low $\varepsilon$, $\omega_{\nabla\beta}^2 \approx c_1 k_\parallel^2 + c_0$, where $c_0$ and $c_1$ are constants that are independent of $q_{\min}$, but may depend on toroidal mode number. It is assumed here that a similar relationship holds between $\omega_{\nabla\beta}^2$ and $k_\parallel$ at high $\beta$ and high $\varepsilon$, although $c_0$ and $c_1$ may differ from the low $\beta$, low $\varepsilon$ case. This assumption may, to a certain extent, be tested by the comparison of the reconstructed $q_{\min}$ with that determined independently using MSE measurements. The resulting relationship between $q_{\min}$ and $\omega$ has a form similar to Eq. (5),

$$q_{\min} = m/(n + \sqrt{\omega^2 - \omega_0^2}/\omega_{\text{slope}}), \tag{6}$$

where $\omega_0$ and $\omega_{\text{slope}}$ are parameters that are expected to depend on $\omega_{\text{geo}}$ and $\omega_A$, respectively. The parameters $\omega_0$ and $\omega_{\text{slope}}$ are also expected to depend on $\nabla\beta$, through the values of $c_0$ and $c_1$, respectively. Figure 7 shows the reconstructed $q_{\min}$.[16] For the purposes of this reconstruction, the value used for $\omega_0$ varies linearly with time. It is determined individually for each mode from the observed minima of the mode frequency. For instance, the value used for the $n=2$ mode is taken to be $2\pi f_{\text{geo}}$, using the value of $f_{\text{geo}}$ is shown in Fig. 3. (Recall that the value shown for $f_{\text{geo}}$ is actually the predicted value, rescaled slightly so that it matches the minima of the observed $n=2$ mode, an adjustment that is within experimental uncertainty.) The value for $\omega_{\text{slope}}$ is taken for all modes to be simply $\omega_A$. (In principle, of course, $\omega_{\text{slope}}$ should depend to some extent on $\nabla\beta$, but $\omega_A$ appears to be a good estimate, as discussed below.) Figure 7 indicates the values of $q_{\min}$ determined from the AC mode frequency minima. These values are determined, as before, using toroidal mode numbers that are measured and poloidal mode numbers that are chosen to produce a smooth variation of $q_{\min}$ with time. Also shown is the reconstruction of $q_{\min}$ at other times using the Doppler corrected mode frequencies of Fig. 3(b). (The colors of the lines correspond to the toroidal mode numbers of the modes used. The poloidal mode numbers used in the reconstruction are indicated by annotations in the figure.) The value of $q_{\min}$ determined using MSE measurements is shown for a similar plasma with a slightly higher density. This value agrees fairly well with the reconstructed value of $q_{\min}$, which tends to support the use of Eq. (6) for the reconstruction and the underlying form assumed for the relationship between $k_\parallel$ and $\omega_{\nabla\beta}^2$. It is also worth noting that, while the value of reconstructed $q_{\min}$ is insensitive to $\omega_{\text{slope}}$ at the frequency minima, it is, in contrast, sensitive to $\omega_{\text{slope}}$ at other times are. This suggests that the assumed value $\omega_A$ is, in fact, a good estimate.

## V. NOVA-K RESULTS

NOVA-K is used to calculate the frequency and structure of an $(n,m)=(2,4)$ Alfvén cascade mode using the plasma geometry and conditions at a time near the end of the plasma current ramp in a moderate $\beta$ NSTX plasma of the type described in Sec. II above. Specifically, the conditions considered are those at $t=0.230$ s of the plasma illustrated in Fig. 1. The calculation is compared to measurements of an $n=2$ AC mode observed in that plasma at that time. The vacuum toroidal magnetic field is $B_T=5.5$ kG at the geometric axis of the plasma, $R=1$ m. At the time of interest, $n_{e0}\sim 2.7\times 10^{19}$ m$^{-3}$, $T_{e0}\sim 1$ keV, $q_{\min}\sim 1.9$, and $\beta_T\sim 3\%$ at $R=1.25$ m, the location of minimum $q$. The ion, electron, and fast-ion pressures are $P_i\sim 1.6$ kPa, $P_e\sim 1.9$ kPa, and $P_f\sim 2.0$ kPa at the location of minimum $q$. LRDFIT is used to model the equilibrium, incorporating MSE measurements. TRANSP is used to model the fast ions, as described in Sec. II above.

In order to incorporate compressional effects, NOVA-K assumes a single ion species plasma and uses the adiabatic equation of state, $P\rho^{-\gamma}=\text{const}$, to constrain the relationship between perturbations of total plasma pressure $P$ and total mass density $\rho$. The value of the plasma adiabatic index $\gamma$ is treated as an input to the calculation. For the conditions considered here, the fast-ion contribution to total pressure is significant, so, to compare NOVA-K calculations with the experiment, a value must be chosen for $\gamma$ that accounts for the compressibility of the fast-ions. However, there is little theoretical guidance in the literature of AC modes regarding the

role of fast-ion compressibility in choosing an appropriate value for $\gamma$. The approach taken for the calculation discussed here is motivated by Ref. 22, which, although it does not consider the influence of fast-ion compressibility, indicates how to determine $\gamma$ in a multiple ion species plasma (i.e., deuterium and tritium). For the calculation discussed here, the fast ions are treated as a second ion species, in addition to the bulk thermal ion species, and $\gamma$ is determined from the relation

$$\gamma P_{\mathrm{tot}} = \gamma_e P_e + \gamma_i P_i + \gamma_f P_f. \tag{7}$$

Based on the work of Berk and Lauber,[43] which considers one thermal ion species and includes kinetic effects with corrections up to order $1/2q^2$, the combined thermal contribution to $\gamma P_{\mathrm{tot}}$ is taken to be

$$\gamma_e P_e + \gamma_e P_i = (1 + 1/2q^2)P_e + 7/4P_i + (9/8q^2)P_i/(P_e/P_i + 7/4). \tag{8}$$

(Detailed calculations of the separate contributions of electrons and ions to $\omega_{\mathrm{geo}}$ are also presented in Refs. 44 and 45.) For the purpose of the analysis presented here, the fast-ion contribution is assumed to be roughly similar to the electron contribution, $\gamma_e P_e = (1+1/2q^2)P_e$ (see Ref. 22), which gives $\gamma_f P_f = (1+1/2q^2)P_f$. This is motivated by the consideration that fast ions move very quickly parallel to the magnetic field, much like electrons, so fast-ion temperature should be isothermal in the parallel direction for perturbations at the frequencies considered, as is electron temperature. The expression in Eq. (7) may then be rewritten as

$$\gamma P_{\mathrm{tot}} = (1 + 1/2q^2)P_f + [(1 + 1/2q^2)P_e + 7/4P_i + (9/8q^2)P_i/(P_e/P_i + 7/4)]. \tag{9}$$

For the plasma conditions for which the NOVA-K calculation is performed, using Eq. (9) gives values of $\gamma$ ranging from 1.34 to 1.38 over the full upward frequency sweep of the $(n,m)=(2,4)$ AC mode.

Notably, although the form assumed for $\gamma$ [Eq. (7)] depends on $\gamma_f$, the resulting prediction for AC mode frequency is not expected to be greatly sensitive to its value under the conditions for which the calculation is performed. A change of $\pm(1+1/2q^2)$ in $\gamma_f$ (i.e., doubling $\gamma_f$ or assuming $\gamma_f=0$) modifies the value $\gamma$ by $\pm 0.41$ or $\sim \pm 30\%$. This changes the predicted value of $\omega_{\mathrm{geo}}$ by only $\sim \pm 15\%$. Furthermore, this change will affect the mode frequency less severely at the end of the upsweep than at the start, given the dependence of mode frequency on $\omega_{\mathrm{geo}}$ [approximately indicated by Eq. (2)]. Consequently, given the other uncertainties involved, such as the uncertainty in the composition of the plasma, the comparison of the NOVA-K results with the experiment for these conditions may yield little insight into the influence of fast-ion compressibility on the AC mode frequency.

Figure 8(a) compares the experimentally observed AC mode frequency with the frequency calculated by NOVA-K for a range of $q_{\mathrm{min}}$ spanning most of the AC mode upward frequency sweep. The calculated frequency is not shown for $q_{\mathrm{min}} > 1.92$ because, as discussed below, strong interaction of the AC modes with the continuum does not allow NOVA-K to find a converged solution for the AC mode. The experimentally observed frequency is Doppler corrected using the toroidal plasma rotation measured by CHERS at the location of minimum $q$. To map the upsweep of the experimental AC mode frequency to $q_{\mathrm{min}}$, $q_{\mathrm{min}}$ is assumed to vary linearly in time from $m/n=2$ to $(m-\frac{1}{2})/n=1.75$. For the NOVA-K calculation, a series of small offsets is applied to the experimental $q$ profile to vary $q_{\mathrm{min}}$ over the range shown. The uncertainties shown for the experimental frequency combine the statistical uncertainty of the Doppler correction and the observed bandwidth of the mode. The experimental mode frequency is determined using a sequence of records 1.0 ms long, overlapping by 0.5 ms. The records are Hanning conditioned and Fourier transformed. No attempt is made to account for the relatively strong radial variation of the toroidal rotation ($\sim\frac{1}{2}$ kHz/cm between the magnetic axis and the location of

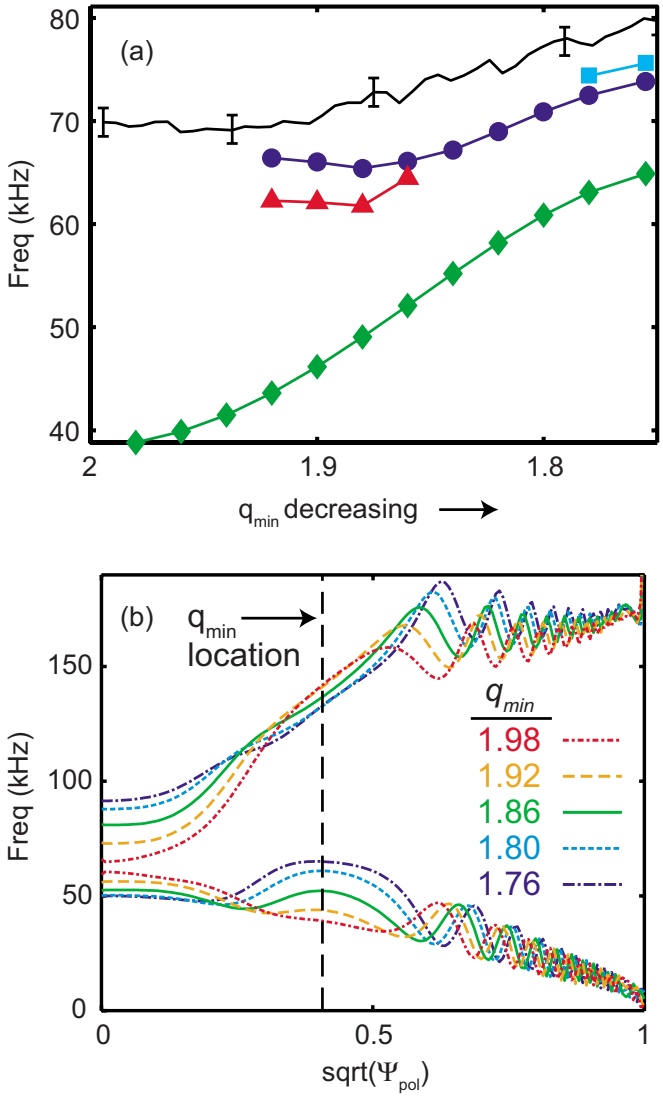


FIG. 8. (Color online) (a) Doppler corrected frequency of experimentally observed $(n,m)=(2,4)$ AC mode (—). Also, NOVA-K calculation of mode frequency (●), and frequency of extra modes resulting from splitting due to coupling with axis-localized AE (▲) and TAE in outboard neighboring local TAE gap (■). Frequency of continuum (♦) calculated by NOVA-K at location of minimum $q$. (b) Upper and lower TAE continua calculated by NOVA-K with $q$ profile adjusted by small offsets to give different values of $q_{\mathrm{min}}$. Location of minimum $q$ is also shown (– –).

minimum $q$), since it is not entirely clear how such rotation shear affects the AC mode. Despite the uncertainty introduced by rotation shear, the experimental frequency is within ~5 kHz of the calculated frequency, which, although greater than the statistical uncertainty of the experimental frequency, is a relatively small difference. It is also within the uncertainty introduced by inexact knowledge of the plasma composition. (Recall that $f_{geo}$ can vary by up to ~20%, depending on whether the plasma ion species is $He^{2+}$ or $D^{+}$.)

The NOVA-K calculation offers insight into the dependence of the AC mode frequency on $\beta$ and $\nabla\beta$. As can be seen in Fig. 8(b), the Alfvén continuum deforms significantly in regions of weak shear as $q_{min}$ changes, including, in particular, in the region around the location of minimum $q$. Figure 8(b) shows the upper and lower TAE continua for several values of $q_{min}$ in the range spanned in Fig. 8(a). Figure 8(a) shows how the frequency of the lower TAE continuum at the location of minimum $q$ changes with $q_{min}$ due to this deformation. Since the AC mode "lives" above the lower continuum at the location of minimum $q$, a decrease in $q_{min}$ raises the lower continuum and increases the AC mode frequency. This dependence on $q_{min}$ corresponds to the $(k_{\|}V_A)^2$ term in the approximate AC mode dispersion relation given by Eq. (2). The lower continuum frequency also depends on $\beta$. The sensitivity of the lower continuum frequency to $\beta$ is illustrated in Fig. 9(a), which shows the upper and lower Alfvén continua for a range of $\beta$ values. [The value of $\beta$ is adjusted by rescaling the pressure profile, shown in Fig. 9(b).] It can be clearly seen that the lower continuum frequency at the location of $q_{min}$ increases as $\beta$ increases. This dependence on $\beta$ corresponds to the $\omega_{geo}^2$ term in Eq. (2). The elevation of the AC mode frequency above the lower continuum is determined primarily by the $\nabla\beta$ effect. This contribution to the AC mode frequency corresponds to the $\omega_{\nabla\beta}^2$ term (and the much smaller $\delta\omega^2$ term) in Eq. (2). The difference between the lower continuum frequency and the AC mode frequency is quite substantial, particularly near the beginning of the frequency sweep ($q_{min}$=2). This indicates that $\nabla\beta$ can play a significant role in setting the AC mode frequency (an observation also made in Ref. 39). Notably, this difference is on the order of $\omega_{geo}$, which tends to diminish the significance of the choice of $\gamma$ in calculating the AC mode frequency for these conditions.

The NOVA-K calculation also offers insight into a physical process that significantly influences the AE mode spectrum, linear mode coupling. Alfvén eigenmodes (AEs) may often be usefully identified as being of a distinct type, such as an AC mode or a TAE. However, in some circumstances the plasma eigenmodes are not identifiable according to these basic types, but are formed by the coupling of multiple parts that are individually identifiable.[46–48] Of course, the individual parts are not, themselves, plasma eigenmodes, even though, for convenience, they may be referred to as "modes" or Alfvén eigenmodes. The effects of such linear coupling are apparent in the results of the NOVA-K calculation reported here. For values of $q_{min}>1.85$, NOVA-K finds two solutions for the AC mode differing slightly in frequency. A comparison of their radial structure indicates that they are actually formed by coupling, with two different parities, between an AC mode and an Alfvén eigenmode localized at the magnetic axis (see Fig. 10 for one solution; other solution not shown). For $q_{min}$ in this range of values, the frequencies of the extra solutions are indicated in Fig. 8(a).

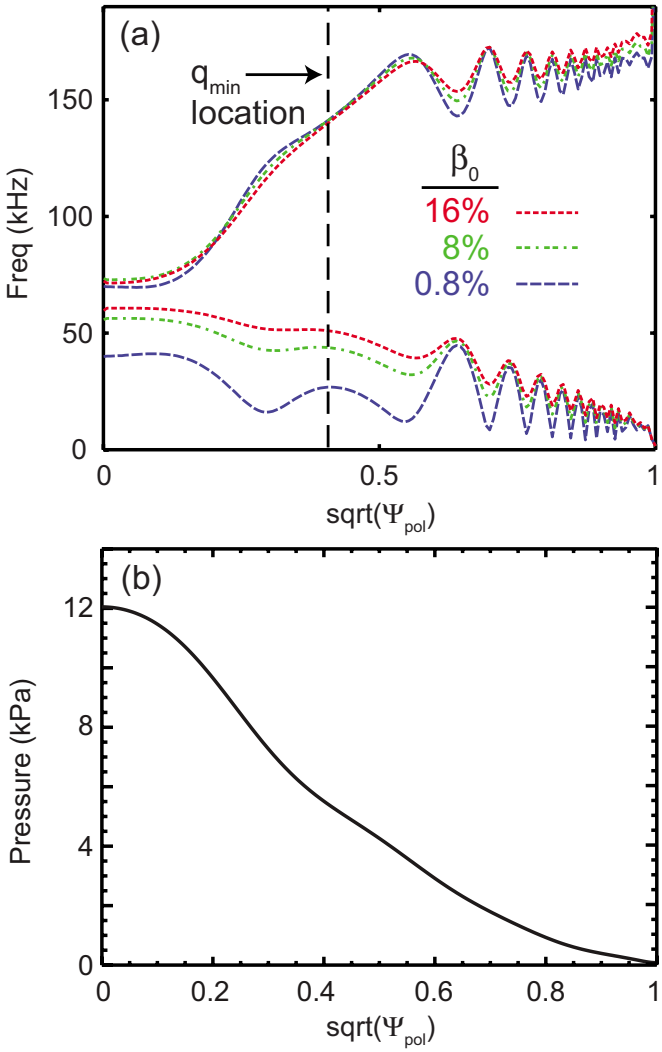


FIG. 9. (Color online) (a) Upper and lower TAE continua calculated by NOVA-K for NSTX with pressure profile rescaled to give different values of $\beta_0$ (same conditions as Fig. 8). Location of minimum $q$ is also shown (– –). (b) Pressure profile used in continuum calculation.

It should be noted that the structures and frequencies of AC mode solutions found for $q_{min}>1.85$ may be significantly influenced by the way in which the $q_{min}$ scan is implemented. The experimental $q$ profile used by NOVA-K has weak shear near the magnetic axis, so the shape of the Alfvén continuum there is very sensitive to the value of $q$ there. For this calculation, since the $q_{min}$ scan is implemented by adding small offsets to the experimental $q$ profile, the continuum deforms substantially near the magnetic axis as $q_{min}$ changes. The characteristics of an AE are generally sensitive to the structure of the continuum where it is localized, so the structure and frequency of the axis-localized AEs coupled to the AC mode will depend on the implementation of the scan. It is important to note, however, that the frequency splitting of the two solutions found for this calculation is proportionally very small. This suggests that, despite the splitting, the cal-

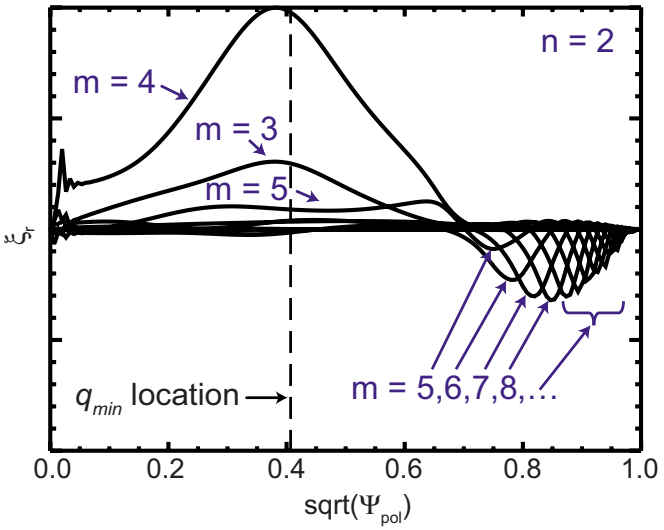


FIG. 10. (Color online) Radial eigenmode structure of the calculated $(n,m)=(2,4)$ AC mode (same mode as Fig. 8) for $q_{\min}=1.86$. The curves are the poloidal components of the radial displacement $(\xi_r)$ of the eigenmode.

culated mode frequency is relatively insensitive to the treatment of the $q$ profile near the magnetic axis.

For values of $q_{\min}<1.79$, NOVA-K finds two solutions with very similar frequencies for the AC mode. A comparison of the radial structures of the two solutions (not shown) indicates that they are formed by coupling, with two different parities, between an AC mode, peaking, as expected, near the minimum in $q$ $[\mathrm{sqrt}(\Psi_{\mathrm{pol}})\approx 0.4]$, and a TAE peaking in the neighboring local TAE gap $[\mathrm{sqrt}(\Psi_{\mathrm{pol}})\approx 0.65]$. The extra frequencies are indicated in Fig. 8(a).

Linear coupling also plays a role in hindering the determination of the AC mode frequency for values of $q_{\min}>1.92$. As noted above, the AC mode frequency is not shown for these values in Fig. 8(a). For values of $q_{\min}$ near the beginning of the frequency sweep $(q_{\min}=2)$, the lower TAE continuum forms a deep well with a small hill at the bottom peaking at the location of $q_{\min}$ [see Fig. 8(b)]. The AC mode is localized around $q_{\min}$, and at its lowest frequency for these values of $q_{\min}$, so it lives in the well. Consequently, the AC mode can intersect the lower continuum, leading to continuum interaction. In fact, it is radially broad enough that, despite being localized, it does so. Continuum interaction causes the AC mode to linearly couple to kinetic Alfvén waves, which have short radial scale structure.[49,50] This short scale structure is not included in the NOVA-K physical model. One consequence of this is that NOVA-K does not converge to a single well-defined solution for the AC mode. Instead, there is an artificial splitting of the AC mode into a large number of solutions with a large range of closely spaced frequencies. Thus, the frequency of the AC mode is not clear at these values of $q_{\min}$.

The radial structure of the eigenmode calculated by NOVA-K for $q_{\min}=1.86$ is illustrated in Fig. 10. The different curves in Fig. 10 are the poloidal components of the radial displacement $(\xi_r)$ of the eigenmode. Inspection of the structure indicates that the eigenmode is formed by an AC mode strongly linearly coupled to a global TAE.[46,48] An AC mode is expected to have a dominant poloidal component $(m=4$, in this case) that peaks in the region of weak shear near the location of minimum $q$ $[\mathrm{sqrt}(\Psi_{\mathrm{pol}})\approx 0.4]$ and weak, but nonvanishing, poloidal sidebands $(m\pm 1=3,5$, in this case) in the weak shear region, as well. The eigenmode clearly has this structure in the region $\mathrm{sqrt}(\Psi_{\mathrm{pol}})<0.7$. A global TAE is usually characterized by a large number of poloidal harmonics concentrated in the increased shear region away from the core.[51,46] As can be seen, the eigenmode has many poloidal components that peak in the region $\mathrm{sqrt}(\Psi_{\mathrm{pol}})>0.7$. Furthermore, the mode frequency lies between the upper and lower TAE continua there, as would be expected for a global TAE. Notably, this strong coupling between the AC mode and the global TAE persists over the full $q_{\min}$ scan illustrated in Fig. 8(a).

The coupling of AC modes with global TAEs also occurs, of course, in conventional tokamaks. Linear coupling between AC modes and global TAEs has been recently observed and modeled using the NOVA-K code in the analysis of DIII-D experiments.[48] However, there is a striking difference between the coupling observed in DIII-D and the coupling of the eigenmode shown in Fig. 10. The coupling in DIII-D is distinctly transitory in nature.[48] It only persists for a brief interval during the frequency sweep of the AC mode. The relatively long persistence of the coupling in NSTX can be explained in part by the higher inverse aspect ratio of NSTX. Significant coupling will only occur if the natural frequencies of the AC mode and global TAE are nearly degenerate.[46,48] The higher inverse aspect ratio of NSTX leads to stronger toroidicity-induced coupling between the parts of the eigenmode. This increases the range of frequency separation for which significant coupling can occur. The AC mode therefore couples to the global TAE over a larger portion of its frequency sweep. The reduced frequency sweep of the NSTX AC mode, which results from higher $\beta$ and $\nabla\beta$, also plays a role. It increases the fraction of the sweep for which the natural frequencies of the AC mode and the global TAE are sufficiently close for significant coupling to occur.

Two fixed frequency quadrature reflectometers operating in O-mode at 30 and 42 GHz (reflecting at $R=1.45$ m and 1.17 m, respectively) are used to measure the structure of the experimental mode. Figure 11 compares these measurements to the reflectometer phase fluctuations that would be expected for the calculated AC mode shown in Fig. 10. Figure 11 shows the profile of the density fluctuation magnitude predicted by NOVA-K along the reflectometer line of site. A "synthetic diagnostic," employing a one-dimensional model of wave propagation along the reflectometer line of site (refraction is neglected), is used to calculate the phase fluctuations this density fluctuation would produce. The magnitude of the expected phase fluctuation is plotted for a range of microwave frequencies versus the major radius of the O-mode cutoff for each frequency. The plotted value, which is normalized in units of density, is given by $|\tilde{\Phi}\nabla n|/2k_v$, where $\tilde{\Phi}$ is the phase fluctuation, $\nabla n$ is the density gradient along the line of site, and $k_v$ is the vacuum microwave wavelength. The magnitude of the phase fluctuation measured by the two reflectometers is also shown. These

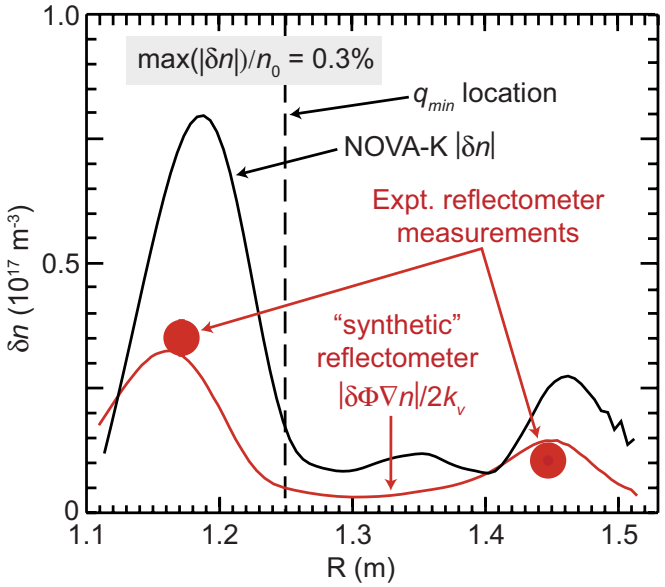


FIG. 11. (Color online) Comparison of NOVA-K calculation with experimentally observed $(n,m)=(2,4)$ AC mode (same mode as Fig. 10). Magnitude of density fluctuation calculated by NOVA-K for along reflectometer line of sight (upper curve) and modeled response using "synthetic" reflectometer (lower curve). Also shown is reflectometer measurement of experimentally observed mode (●). Statistical uncertainty of experimental measurement is size of plot symbol. Location of minimum $q$ is also shown (– –).

values are $|\tilde{\Phi}\nabla n|/2k_v n_0=0.04\%$ at $R=1.45$ m and 0.13% at $R=1.17$ m, where $n_0=2.7\times10^{19}$ m$^{-3}$ is the central plasma density. The statistical uncertainties of the two measurements are indicated by the size of the plot symbols. The scale of the NOVA-K eigenmode is adjusted to give the best least-squared fit between the magnitude of the expected phase fluctuation and the two measurements. This gives a peak density fluctuation level of $|\delta n|/n_0=0.3\%$ at $R=1.19$ m for the eigenmode. As can be seen, the magnitudes of the two measurements are in reasonable agreement with the phase fluctuation magnitude expected from the modeling of the NOVA-K mode structure.

The AC mode fluctuations detected by the two reflectometers not only differ in amplitude, they are out of phase by 0.46 $\pi$ radians. This relative phase differs significantly from the value of 1.03 $\pi$ radians expected from the modeled NOVA-K mode structure. There are at least two possible explanations for this. First, the reflectometer modeling neglects two- or three-dimensional wave propagation effects that may influence the relative phase of the two measurements. Refraction is also ignored, although the experimental setup is designed to minimize its effect. The microwave antennae are located near the midplane, where the curvature of the constant density surfaces is weak, and they are angled to launch and receive in a direction approximately normal to the plasma surface. Second, NOVA-K may be missing some physics that affects the relative phase. Candidates include toroidal rotation, kinetic effects, and up-down asymmetry in the equilibrium (e.g., the plasma is operated with a lower single null divertor). As discussed above, the eigenmode calculated by NOVA-K is an AC mode linearly coupled to a global TAE. The 42 GHz measurement is localized to the region near the location of minimum $q$, where the eigenmode has predominantly the structure of an AC mode. The 30 GHz measurement, in contrast, is localized to the edge, where the eigenmode has predominantly the structure of a global TAE. Consequently, the relative phase between the two measurements will be sensitive to the details of the coupling, which may be influenced by some of the physics effects not included in NOVA-K.

## VI. DISCUSSION

One of the key challenges in the study of Alfvén cascade modes is to understand why they are not commonly observed during normal reverse-shear operation in spherical tori. AC modes potentially have both beneficial and deleterious effects, making control and stabilization of AC modes desirable capabilities. The recent observation of AC modes in low $\beta$ plasmas in spherical tori has prompted the conjecture that there is a $\beta$ threshold for suppression of AC modes that explains their absence during normal operation.[16] However, theoretical treatments of the AC mode at low $\varepsilon$ and $\beta$ have indicated that role of $\beta$ in determining the stability and properties of the AC mode is complex, and that $\nabla\beta$ also plays a role. Both $\beta$ and $\nabla\beta$ are shown to affect the relative size of the AC mode frequency sweep. In particular, increases in the magnitudes of both quantities can reduce the relative size of the frequency sweep. This raises the question of whether the lack of observation of AC modes in normal operation results simply from a lack of recognition, since the frequency sweep is one of most obvious identifying features of AC modes. However, theory has also indicated a direct role for $\nabla\beta$ in the suppression of AC modes. As the magnitude of $\nabla\beta$ increases, the frequency of an AC mode near the end of its sweep is depressed, until eventually it moves into the lower continuum, leading to continuum damping[34,23,24] and potential stabilization of the mode. This stabilization at the end of the sweep can extend to cover a larger fraction of the sweep as $|\nabla\beta|$ increases. It is not clear from theory whether $\beta$ also plays a direct role in the stabilization of AC modes.

Another key challenge in the study of Alfvén cascade modes is to understand the influence of fast-ion compressibility in the coupling of AC modes to acoustic oscillations. NOVA-K is a powerful tool for addressing this challenge. Comparison of NOVA-K predictions with experiments allows, in principle, characterizing this influence in terms of a single overall plasma adiabatic index $\gamma$. As noted above, there is little theoretical guidance in the literature of AC modes regarding the role of fast-ion compressibility in determining the value for $\gamma$. However, recent efforts to compare observations of Alfvén eigenmodes (including AC modes) with NOVA-K calculations in the DIII-D tokamak have addressed this issue empirically.[52] The plasmas considered had an on-axis thermal (ion+electron) $\beta$ of 0.7% (Ref. 52) and $P_f\sim(P_e+P_i)$ at the location of minimum $q$.[53] Both the electron density $(\delta n_e)$ and temperature $(\delta T_e)$ perturbation structures were compared to the structures predicted using NOVA-K. This comparison of both fluctuating quantities was deemed important, since the value of the ratio $\delta n_e/\delta T_e$ determined from the NOVA-K calculation was expected to be

sensitive to the value chosen for $\gamma$.[52] The predictions proved to be consistent with the experimental observations assuming $\gamma=5/3$, the canonical value for an ideal gas with 3 degrees of freedom. Values of $\gamma$ over a range of 0 to 2 were tried to test the sensitivity of this comparison to the value of $\gamma$. It was found that, in fact, the NOVA-K predictions were consistent with the experimental observations for values ranging from 1.2 to 1.8.

As discussed above, the approach to calculating $\gamma$ used for the NOVA-K calculation discussed here, motivated by Ref. 22, is expressed in Eq. (7). However, further consideration leads to an arguably more appropriate approach to determining $\gamma$. The relationship between adiabatic fluctuations in total mass density $\rho_{\mathrm{tot}}$ and total pressure is

$$\gamma\delta\rho_{\mathrm{tot}}/\rho_{\mathrm{tot}} = \delta P_{\mathrm{tot}}/P_{\mathrm{tot}}. \tag{10}$$

In contrast with the expression in Eq. (7), this relationship implies a value for $\gamma$ that is very insensitive to $\gamma_f$ for a value of $\gamma_f$ of order unity when $n_f/n_e \ll 1$ and $T_e/T_f \ll 1$ (where $T_f \equiv P_f/n_f$ is an effective fast-ion temperature). These are conditions that are typically satisfied in a broad range of tokamak experiments. Neglecting fast-ion inertia, the adiabatic response of the fast-ion density perturbation $\delta n_f$ to an electrostatic perturbation $\delta\phi$ is given by

$$\delta n_f \approx -eZ_f n_f \delta\phi/\gamma_f T_f, \tag{11}$$

where $Z_f$ is the fast-ion atomic number. Since the response of the electron density perturbation is given by $\delta n_e \approx e n_e \delta\phi/T_e$, it can seen that

$$\delta n_f \approx -(Z_f/\gamma_f)(T_e/T_f)(n_f/n_e)\delta n_e. \tag{12}$$

So, if $\gamma_f$ is of order unity, $n_f/n_e \ll 1$ and $T_e/T_f \ll 1$, then $\delta n_f \ll \delta n_e$. This, in turn, implies $Z_i \delta n_i \approx \delta n_e$, $\delta\rho_{\mathrm{tot}} \approx m_i \delta n_i$, and $|\delta P_f/\delta P_e| \approx (Z_f/\gamma_f)(n_f/n_e) \ll 1$. In addition, $n_f/n_e \ll 1$ implies $\rho_{\mathrm{tot}} \approx m_i n_i$. Consequently, Eq. (10) gives

$$\begin{aligned}\gamma &= (\delta P_{\mathrm{tot}}/\delta\rho_{\mathrm{tot}})(\rho_{\mathrm{tot}}/P_{\mathrm{tot}}) \\ &\approx [(\gamma_e \delta n_e T_e + \gamma_i \delta n_i T_i)/\delta n_i](n_i/P_{\mathrm{tot}}) \\ &= (\gamma_e P_e + \gamma_i P_i)/P_{\mathrm{tot}},\end{aligned} \tag{13}$$

where $P_{\mathrm{tot}}$, of course, includes $P_f$. Interestingly, inspection of Eqs. (7) and (13) shows that Eq. (13) coincidently gives the same value for $\gamma$ as would Eq. (7) under the assumption $\gamma_f=0$. Of course, the ordering $\delta n_f \ll \delta n_e$ that leads to Eq. (13) fails if $\gamma_f$ approaches 0. The value of $\gamma$ resulting from this analysis for the conditions of the NOVA-K calculation discussed here is ~0.95, or ~30% less than that actually used for the NOVA-K calculation. Unfortunately, as discussed above, a reduction of $\gamma$ by this amount leads to a reduction of the AC mode frequency of less than 15%, so, given the other uncertainties involved, these experimental conditions do not permit a strong comparative test of Eqs. (7) and (13).

It should be noted that the question of how fast-ion compressibility influences the AC mode frequency may be moot for high $n$ AC modes at the lower, but still nonvanishing, values of $\beta$ achievable in conventional tokamaks. The AC mode frequency is relatively insensitive to $\gamma$ for these modes.[39] NOVA-K calculations for the JET tokamak were performed for values of $\gamma$ ranging from 0 to 2. There was a significant variation in frequency (~40%) over this range for the $n=1$ AC mode, but the for the $n=2$, there was a much smaller variation (~25%) and for the $n=3$, there was an even smaller variation (~10%).

One particularly interesting result of the NOVA-K calculations discussed here is the extensive degree to which the eigenmode is formed by coupling between an AC mode and other AEs, including, in particular, a global TAE. Although the calculation discussed here focuses on a specific set of plasma conditions, such coupling may arguably be expected to occur more frequently and with greater strength in spherical tori (when AC modes are unstable, of course) than in conventional tokamaks. The factors at work in the conditions discussed here represent relatively robust differences between spherical tori and conventional tokamaks. Not only is the higher inverse aspect ratio, and subsequent stronger toroidicity-induced coupling, a constant factor in spherical tori, the size of AC mode frequency sweeps will be significantly reduced much more commonly in spherical tori than in conventional tokamaks. There is also another factor that will tend to favor such coupling in spherical tori more than in conventional tokamaks. The linear coupling of AC modes with other types of AEs will, in general, tend to create eigenmodes with a large radial extent. Such eigenmodes may be more susceptible than eigenmodes consisting of uncoupled AC modes to intersect the continuum and consequently be stabilized by continuum interaction. The higher inverse aspect ratio and higher typical $\beta$ of spherical tori will both tend to reduce the likelihood for such continuum intersection in spherical tori. A higher inverse aspect ratio widens the gap between the upper and lower TAE continua, in part by lowering the peaks in the lower continuum. A higher $\beta$ raises the natural frequency of the AC mode, potentially elevating the eigenmode into the gap. Of course, it must be noted that spherical tori tend to have higher $|\nabla\beta|$ as well as higher $\beta$, and the effect of higher $|\nabla\beta|$ is more complicated. A higher $|\nabla\beta|$ elevates the AC mode frequency near the beginning of the sweep, much like a higher $\beta$. However, it lowers the frequency near the end of sweep. This reduction near the end of the sweep potentially prevents the AC mode frequency from ever rising above the lower continuum.[34,23,24]

The potentially greater strength and more frequency occurrence of linear coupling between AC modes and other AEs in spherical tori has at least two important implications. First, eigenmodes with broad poloidal spectra resulting from such coupling may be more efficient at redistributing, and, in particular, deconfining fast ions than narrower spectrum eigenmodes that are purely AC modes, TAEs, or global TAEs. AEs have been shown theoretically[54,55] and experimentally[36,37] to be capable of very efficiently transporting and deconfining fast ions through a process of multimode phase-space resonance overlap. An individual AE traps fast-ions in a region of phase-space surrounding an orbit that is resonant with the AE. When the trapped regions of multiple modes overlap, stochastic fast-ion trajectories result. The excitation of a single eigenmode with a broad poloidal spectrum should have the same effect as the simultaneous independent excitation of multiple narrow spectrum

modes, increasing the likelihood that such transport will occur. Thus, this fast-ion transport mechanism is potentially more significant in spherical tori than in conventional tokamaks. The second implication of ready coupling arises from the coupling between AC modes and AEs with large edge-peaking components, such as global TAEs, for the experimental observation of AC modes. Mirnov coils positioned outside the plasma have proven to be invaluable tools for studying the activity of many types of AEs in toroidal plasmas. In contrast, the study of AC modes in conventional tokamaks has largely shown such coils to be relatively insensitive to AC modes.[56,57] However, the coupling of AC modes to AEs with strong edge-peaking components has been shown to result in a relatively strong magnetic perturbation at the edge of the plasma.[48] Consequently, more ready coupling in spherical tori will tend to make Mirnov coils outside the plasma much more for useful in studying ACs in spherical tori than in conventional tokamaks.

## VII. SUMMARY

In summary, AC modes are identified in NSTX L-mode plasmas over a range of $\beta$ values, including low values ($\beta_T \sim 6\%$) that are comparable to those achievable in conventional tokamaks, as well as higher values that are nonetheless still low for NSTX ($\beta_T \sim 11\%$). A reduction of the relative size of the AC frequency sweep is observed with increasing $\beta$. AC modes are not observed at very high $\beta$ (i.e., normal NSTX $\beta$).[16] The trend in relative sweep size with $\beta$ raises the possibility that this may be because AC modes may not be recognized at sufficiently high $\beta$ even though they may still be unstable. Measurements with the sFLIP diagnostic indicate that AC modes play a role in the loss of fast-ions from the plasma and AC mode polarization measured at the plasma edge is consistent with expectation for a shear Alfvén wave radially localized to the minimum of $q$. MHD spectroscopy is also tested and shown to be usable even at high $\beta$ (i.e., $\beta_T \sim 11\%$).

Observations of AC modes over the range of $\beta$ presented here are consistent with theory. In particular, changes observed in the AC mode spectrum with increasing $\beta$ are consistent with predicted $\beta$ and $\nabla\beta$ effects, including a significant reduction in the relative size of the frequency sweep and a toroidal mode number dependence in the minimum mode frequency. Additionally, the structure and frequency of an observed AC mode at low $\beta$ (i.e., $\beta_T \sim 3\%$) are directly compared with those calculated by NOVA-K for the same equilibrium conditions and shown to be consistent. The results of the NOVA-K calculation have further implications. The calculation indicates that the change in mode frequency due to $\nabla\beta$ can contribute significantly to frequency sweep reduction, on the same order as the change due $\beta$ (i.e., the contribution of $\omega_{\text{geo}}$ to mode frequency). Furthermore, the structure of the calculated eigenmode is significantly influenced by linear coupling between the AC mode and other AEs. Such coupling will arguably occur more frequently and with greater strength in spherical tori than in conventional tokamaks. This is significant since such coupling results in eigenmodes that have a broader poloidal spectrum than an uncoupled AC mode, possibly leading to very efficient fast-ion transport due to phase space resonance overlap and enhancing the utility of edge Mirnov coils in the study of AC modes.

## ACKNOWLEDGEMENTS

This work is supported by U.S. DOE Contract Nos. DE-FG03-99ER54527 and DE-AC02-76CH03073.

[1] M. Ono, S. M. Kaye, Y.-K. M. Peng, G. Barnes, W. Blanchard, M. D. Carter, J. Chrzanowski, L. Dudek, R. Ewig, D. Gates, R. E. Hatcher, T. Jarboe, S. C. Jardin, D. Johnson, R. Kaita, M. Kalish, C. E. Kessel, H. W. Kugel, R. Maingi, R. Majeski, J. Manickam, B. McCormack, J. Menard, D. Mueller, B. A. Nelson, B. E. Nelson, C. Neumeyer, G. Oliaro, F. Paoletti, R. Parsells, E. Perry, N. Pomphrey, S. Ramakrishnan, R. Raman, G. Rewoldt, J. Robinson, A. L. Roquemore, P. Ryan, S. Sabbagh, D. Swain, E. J. Synakowski, M. Viola, M. Williams, J. R. Wilson, and NSTX Team, Nucl. Fusion **40**, 557 (2000).
[2] ITER Physics Basis Editors, ITER Expert Group Chairs and Co-Chairs, and ITER Joint Central and Physics Integration Unit, Nucl. Fusion **39**, 2137 (1999).
[3] E. J. Doyle, A. M. Garofalo, C. M. Greenfield, S. M. Kaye, J. E. Menard, M. Murakami, S. A. Sabbagh, M. E. Austin, R. E. Bell, K. H. Burrell, J. R. Ferron, D. A. Gates, R. J. Groebner, A. W. Hyatt, R. J. Jayakumar, J. E. Kinsey, B. P. LeBlanc, T. C. Luce, G. R. McKee, M. Okabayashi, Y.-K. M. Peng, C. C. Petty, P. A. Politzer, T. L. Rhodes, M. R. Wade, R. E. Waltz, and the DIII-D and NSTX Research Teams, Plasma Phys. Controlled Fusion **48**, B39 (2006).
[4] M. Takechi, A. Fukuyama, M. Ishikawa, C. Z. Cheng, K. Shinohara, T. Ozeki, Y. Kusama, S. Takeji, T. Fujita, T. Oikawa, T. Suzuki, N. Oyama, A. Morioka, N. N. Gorelenkov, G. J. Kramer, R. Nazikian, and the JT-60 Team, Phys. Plasmas **12**, 082509 (2005).
[5] M. Ishikawa, M. Takechi, K. Shinohara, Y. Kusama, G. Matsunaga, V. A. Krasilnikov, Yu. Kashuck, M. Isobe, T. Nishitani, A. Morioka, M. Sasao, C. Z. Cheng, N. N. Gorelenkov, G. J. Kramer, R. Nazikian, and the JT-60 Team, Nucl. Fusion **46**, S898 (2006).
[6] W. W. Heidbrink, N. N. Gorelenkov, Y. Luo, M. A. Van Zeeland, R. B. White, M. E. Austin, K. H. Burrell, G. J. Kramer, M. A. Makowski, G. R. McKee, R. Nazikian, and the DIII-D Team, Phys. Rev. Lett. **99**, 245002 (2007).
[7] M. A. Van Zeeland, W. W. Heidbrink, R. Nazikian, W. M. Solomon, M. E. Austin, H. L. Berk, N. N. Gorelenkov, C. T. Holcomb, A. W. Hyatt, G. J. Kramer, J. Lohr, M. A. Makowski, G. R. McKee, C. C. Petty, S. E. Sharapov, and T. L. Rhodes, Plasma Phys. Controlled Fusion **50**, 035009 (2008).
[8] H. Kimura, Y. Kusama, M. Saigusa, G. J. Kramer, K. Tobita, M. Nemoto, T. Kondoh, T. Nishitani, O. da Costa, T. Ozeki, T. Oikawa, S. Moriyama, A. Morioka, G. Y. Fu, C. Z. Cheng, and V. I. Afanas'ev, Nucl. Fusion **38**, 1303 (1998).
[9] S. E. Sharapov, D. Testa, B. Alper, D. N. Borba, A. Fasoli, N. C. Hawkes, R. F. Heeter, M. J. Mantsinen, and M. von Hellermann, Phys. Lett. A **289**, 127 (2001).
[10] R. Nazikian, G. J. Kramer, C. Z. Cheng, N. N. Gorelenkov, H. L. Berk, and S. E. Sharapov, Phys. Rev. Lett. **91**, 125003 (2003).
[11] J. A. Snipes, N. Basse, C. Boswell, E. Edlund, A. Fasoli, N. N. Gorelenkov, R. S. Granetz, L. Lin, Y. Lin, R. Parker, M. Porkolab, J. Sears, S. Sharapov, V. Tang, and S. Wukitch, Phys. Plasmas **12**, 056102 (2005).
[12] M. A. Van Zeeland, G. J. Kramer, M. E. Austin, R. L. Boivin, W. W. Heidbrink, M. A. Makowski, G. R. McKee, R. Nazikian, W. M. Solomon, and G. Wang, Phys. Rev. Lett. **97**, 135001 (2006).
[13] A. Fasoli, D. Testa, S. Sharapov, H. L. Berk, B. Breizman, A. Gondhalekar, R. F. Heeter, M. Mantsinen, and Contributors to the EFDA-JET Workprogramme, Plasma Phys. Controlled Fusion **44**, B159 (2002).
[14] S. E. Sharapov, B. Alper, H. L. Berk, D. N. Borba, B. N. Breizman, C. D. Challis, A. Fasoli, N. C. Hawkes, T. C. Hender, J. Mailloux, S. D. Pinches, and D. Testa, Phys. Plasmas **9**, 2027 (2002).
[15] S. D. Pinches, R. J. Akers, L. C. Appel, R. J. Buttery, I. Chapman, N. Conway, G. Cunningham, M. P. Gryaznevich, T. C. Hender, D. F. Howell, G. T. A. Huysmans, R. Martin, and S. E. Sharapov, in Proceedings of the 21st IAEA Conference, Chengdu, 16–21 October 2006, EX/7-2Ra (http://www-naweb.iaea.org/napc/physics/FEC/FEC2006/html/index.htm).

[16]E. D. Fredrickson, N. A. Crocker, N. N. Gorelenkov, W. W. Heidbrink, S. Kubota, F. M. Levinton, H. Yuh, J. E. Menard, and R. E. Bell, Phys. Plasmas **14**, 102510 (2007).
[17]F. M. Levinton, H. Yuh, M. G. Bell, R. E. Bell, L. Delgado-Aparicio, M. Finkenthal, E. D. Fredrickson, D. A. Gates, S. M. Kaye, B. P. LeBlanc, R. Maingi, J. E. Menard, D. Mikkelsen, D. Mueller, R. Raman, G. Rewoldt, S. A. Sabbagh, D. Stutman, K. Tritz, and W. Wang, Phys. Plasmas **14**, 056119 (2007).
[18]M. G. Bell, R. E. Bell, D. A. Gates, S. M. Kaye, H. Kugel, B. P. LeBlanc, F. M. Levinton, R. Maingi, J. E. Menard, R. Raman, S. A. Sabbagh, D. Stutman, and the NSTX Research Team, Nucl. Fusion **46**, S565 (2006).
[19]H. L. Berk, D. N. Borba, B. N. Breizman, S. D. Pinches, and S. E. Sharapov, Phys. Rev. Lett. **87**, 185002 (2001).
[20]F. Zonca, S. Briguglio, L. Chen, S. Dettrick, G. Fogaccia, D. Testa, and G. Vlad, Phys. Plasmas **9**, 4939 (2002).
[21]B. N. Breizman, H. L. Berk, M. S. Pekker, S. D. Pinches, and S. E. Sharapov, Phys. Plasmas **10**, 3649 (2003).
[22]B. N. Breizman, M. S. Pekker, S. E. Sharapov, and JET EFDA Contributors, Phys. Plasmas **12**, 112506 (2005).
[23]N. N. Gorelenkov, G. J. Kramer, and R. Nazikian, Plasma Phys. Controlled Fusion **48**, 1255 (2006).
[24]G. Y. Fu and H. L. Berk, Phys. Plasmas **13**, 052502 (2006).
[25]C. Z. Cheng and M. S. Chance, J. Comput. Phys. **71**, 124 (1987).
[26]C. Z. Cheng, Phys. Rep. **211**, 1 (1992).
[27]N. N. Gorelenkov, C. Z. Cheng, and G. Y. Fu, Phys. Plasmas **6**, 2802 (1999).
[28]M. S. Chu, J. M. Greene, L. L. Lao, A. D. Turnbull, and M. S. Chance, Phys. Fluids B **4**, 3713 (1992).
[29]J. P. H. E. Ongena, M. Evrard, and D. McCune, Fusion Sci. Technol. **53**, 367 (2008).
[30]R. V. Budny, Nucl. Fusion **34**, 1247 (1994).
[31]D. Johnson and the NSTX Team, Plasma Phys. Controlled Fusion **45**, 1975 (2003).
[32]R. E. Bell, B. P. LeBlanc, C. Bourdelle, D. R. Ernst, E. D. Fredrickson, D. A. Gates, J. C. Hosea, D. W. Johnson, S. M. Kaye, R. Maingi, S. Medley, J. E. Menard, D. Mueller, M. Ono, F. Paoletti, M. Peng, S. A. Sabbagh, D. Stutman, D. W. Swaina, E. J. Synakowski, and J. R. Wilson, Europhys. Conf. Abstr. **25A**, 1021 (2001).
[33]B. P. LeBlanc, R. E. Bell, D. W. Johnson, D. E. Hoffman, D. C. Long, and R. W. Palladino, Rev. Sci. Instrum. **74**, 1659 (2003).
[34]G. J. Kramer, N. N. Gorelenkov, R. Nazikian, and C. Z. Cheng, Plasma Phys. Controlled Fusion **46**, L23 (2004).
[35]D. S. Darrow, Rev. Sci. Instrum. **79**, 023502 (2008).
[36]E. D. Fredrickson, R. E. Bell, D. S. Darrow, G. Y. Fu, N. N. Gorelenkov, B. P. LeBlanc, S. S. Medley, J. E. Menard, H. Park, A. L. Roquemore, W. W. Heidbrink, S. A. Sabbagh, D. Stutman, K. Tritz, N. A. Crocker, S. Kubota, W. Peebles, K. C. Lee, and F. M. Levinton, Phys. Plasmas **13**, 056109 (2006).
[37]E. D. Fredrickson, N. N. Gorelenkov, R. E. Bell, J. E. Menard, A. L. Roquemore, S. Kubota, N. A. Crocker, and W. Peebles, Nucl. Fusion **46**, S926 (2006).
[38]N. Winsor, J. L. Johnson, and J. M. Dawson, Phys. Fluids **11**, 2448 (1968).
[39]G. J. Kramer, R. Nazikian, B. Alper, M. de Baar, H. L. Berk, G.-Y. Fu, N. N. Gorelenkov, G. McKee, S. D. Pinches, T. L. Rhodes, S. E. Sharapov, W. M. Solomon, M. A. van Zeeland, and JET EFDA Contributors, Phys. Plasmas **13**, 056104 (2006).
[40]S. E. Sharapov, B. Alper, Yu. F. Baranov, H. L. Berk, D. Borba, C. Boswell, B. N. Breizman, C. D. Challis, M. de Baar, E. De La Luna, E. A. Evangelidis, S. Hacquin, N. C. Hawkes, V. G. Kiptily, S. D. Pinches, P. Sandquist, I. Voitsekhovich, N. P. Young, and JET-EFDA Contributors, Nucl. Fusion **46**, S868 (2006).
[41]M. A. Van Zeeland, M. E. Austin, T. N. Carlstrom, T. Deterly, D. K. Finkenthal, C. T. Holcomb, R. J. Jayakumar, G. J. Kramer, M. A. Makowski, G. R. McKee, R. Nazikian, W. A. Peebles, T. L. Rhodes, W. M. Solomon, and E. J. Strait, Nucl. Fusion **46**, S880 (2006).
[42]M. Porkolab, E. Edlund, L. Lin, R. Parker, C. Rost, J. Sears, J. Snipes, S. J. Wukitch, B. Breizman, N. Gorelenkov, G. J. Kramer, A. Fasoli, and H. Smith, in Proceedings of the 21st IAEA Conference, Chengdu, 16–21 October 2006, EX/P6-16 (http://www-naweb.iaea.org/napc/physics/FEC/FEC2006/html/index.htm).
[43]H. L. Berk and P. Lauber, private communication (2008).
[44]F. Zonca, L. Chen, and R. A. Santoro, Plasma Phys. Controlled Fusion **38**, 2011 (1996).
[45]H. Sugama and T.-H. Watanabe, Phys. Plasmas **13**, 012501 (2006).
[46]G. J. Kramer, C. Z. Cheng, G. Y. Fu, Y. Kusama, R. Nazikian, T. Ozeki, and K. Tobita, Phys. Rev. Lett. **83**, 2961 (1999).
[47]N. P. Young, S. E. Sharapov, V. M. Nakariakov, and JET EFDA Contributors, Plasma Phys. Controlled Fusion **48**, 295 (2006).
[48]M. A. Van Zeeland, M. E. Austin, N. N. Gorelenkov, W. W. Heidbrink, G. J. Kramer, M. A. Makowski, G. R. McKee, R. Nazikian, E. Ruskov, and A. D. Turnbull, Phys. Plasmas **14**, 056102 (2007).
[49]A. Hasegawa and L. Chen, Phys. Rev. Lett. **35**, 370 (1975).
[50]R. R. Mett and S. M. Mahajan, Phys. Fluids B **4**, 2885 (1992).
[51]G. Y. Fu, C. Z. Cheng, R. Budny, Z. Chang, D. S. Darrow, E. Fredrickson, E. Mazzucato, R. Nazikian, K. L. Wong, and S. Zweben, Phys. Plasmas **3**, 4036 (1996).
[52]M. A. Van Zeeland, G. J. Kramer, M. E. Austin, R. L. Boivin, W. W. Heidbrink, M. A. Makowski, G. R. McKee, R. Nazikian, W. M. Solomon, and G. Wang, Phys. Rev. Lett. **97**, 135001 (2006).
[53]M. A. Van Zeeland, private communication (2008).
[54]H. L. Berk, B. N. Breizman, and H. Ye, Phys. Rev. Lett. **68**, 3563 (1992).
[55]A. Fasoli, C. Gormenzano, H. L. Berk, B. Breizman, S. Briguglio, D. S. Darrow, N. Gorelenkov, W. W. Heidbrink, A. Jaun, S. V. Konovalov, R. Nazikian, J.-M. Noterdaeme, S. Sharapov, K. Shinohara, D. Testa, K. Tobita, Y. Todo, G. Vlad, and F. Zonca, Nucl. Fusion **47**, S264 (2007).
[56]S. E. Sharapov, B. Alper, J. Fessey, N. C. Hawkes, N. P. Young, R. Nazikian, G. J. Kramer, D. N. Borba, S. Hacquin, E. De La Luna, S. D. Pinches, J. Rapp, D. Testa, and JET-EFDA Contributors, Phys. Rev. Lett. **93**, 165001 (2004).
[57]R. Nazikian, G. J. Kramer, C. Z. Cheng, N. N. Gorelenkov, H. L. Berk, and S. E. Sharapov, Phys. Rev. Lett. **91**, 125003 (2003).